Chemical Science

ROYAL SOCIETY OF CHEMISTRY

EDGE ARTICLE

View Article Online
View Journal | View Issue

Cite this: *Chem. Sci.*, 2024, **15**, 528

All publication charges for this article have been paid for by the Royal Society of Chemistry

A high-spin alkylperoxo–iron(III) complex with *cis*-anionic ligands: implications for the superoxide reductase mechanism†

Tarali Devi, [ab] Kuheli Dutta,[a] Jennifer Deutscher, [a] Stefan Mebs, [c] Uwe Kuhlmann,[d] Michael Haumann,[c] Beatrice Cula,[a] Holger Dau, [c] Peter Hildebrandt [d] and Kallol Ray *[a]

Received 20th October 2023
Accepted 5th December 2023

DOI: 10.1039/d3sc05603a

rsc.li/chemical-science

The N_3O macrocycle of the 12-TMCO ligand stabilizes a high spin ($S = 5/2$) $[Fe^{III}(12\text{-TMCO})(OO^tBu)Cl]^+$ (**3**-Cl) species in the reaction of $[Fe^{II}(12\text{-TMCO})(OTf)_2]$ (**1**-$(OTf)_2$) with *tert*-butylhydroperoxide (^{t}BuOOH) in the presence of tetraethylammonium chloride (NEt_4Cl) in acetonitrile at −20 °C. In the absence of NEt_4Cl the oxo–iron(IV) complex **2** $[Fe^{IV}(12\text{-TMCO})(O)(CH_3CN)]^{2+}$ is formed, which can be further converted to **3**-Cl by adding NEt_4Cl and ^{t}BuOOH. The role of the *cis*-chloride ligand in the stabilization of the Fe^{III}–OO^tBu moiety can be extended to other anions including the thiolate ligand relevant to the enzyme superoxide reductase (SOR). The present study underlines the importance of subtle electronic changes and secondary interactions in the stability of the biologically relevant metal–dioxygen intermediates. It also provides some rationale for the dramatically different outcomes of the chemistry of iron(III)peroxy intermediates formed in the catalytic cycles of SOR (Fe–O cleavage) and cytochrome P450 (O–O bond lysis) in similar N_4S coordination environments.

Introduction

Iron(III)–hydroperoxo (Fe^{III}–OOH) and iron(III)–alkylperoxo (Fe^{III}–OOR) species have been identified as key intermediates in heme and non-heme iron enzymes.[1–10] In the non-heme enzyme superoxide reductase (SOR), the $[Fe^{III}(His)_4(Cys)OOH]$ intermediate undergoes a proton-mediated Fe–O bond cleavage to release H_2O_2. In contrast, the $[Fe^{III}$(protoporphyrin-IX)(Cys)OOR(H)] intermediate in the heme protein cytochrome P450 (P-450) undergoes O–O bond cleavage to generate a high-valent iron–oxido species, which is then used in a number of hydrogen atom transfer (HAT) and oxygen atom transfer (OAT) reactions. The different fate of the Fe^{III}–OOR(H) intermediates in an otherwise similar N_4S coordination frame has been rationalized based on the different spin states of the Fe^{III}–OOR intermediates in SOR and P-450. The electron donation from a thiolate ligand in SOR is proposed to increase the lifetime of the high-spin (HS) iron(III)–hydroperoxo species to allow its protonation and subsequent release of H_2O_2. In contrast, the "push" of electron density from the *trans*-thiolate ligand is believed to assist in the O–O bond cleavage step in the low-spin (LS) iron(III)–hydroperoxo species in P-450 leading to the generation of the iron(IV)oxo porphyrin cation radical species. The speculated role of the spin-state ($S = 1/2$ *vs.* 5/2) of the iron(III)–hydroperoxo species in controlling the Fe–O *vs.* O–O bond cleavage step is, however, challenged in biomimetic studies, where both HS and LS Fe^{III}–OOR(H) species are found to be amenable to O–O bond lysis in the presence of Lewis bases occupying the 6th coordination site of the Fe(III)–OOR species in both *cis*- and *trans*- orientations.[11–18] Furthermore, recent theoretical[19] and experimental[20,21] studies have also raised the possibility of the presence of a low-spin intermediate with a weak Fe–O bond in the course of O_2 reduction by SOR. Thus, the factors that account for the dramatically different outcomes of the chemistry of SOR *versus* P-450 in similar N_4S coordination environment remain to be determined.

In our effort to understand nature's rationale for using similar active sites for apparently opposite functions, we now report the synthesis and characterization of $S = 5/2$ $[Fe^{III}(12\text{-TMCO})(OOR)L']^+$ (R = -^{t}Bu, -Cumene; $L' = MePhS^-$, F^-, Cl^-, Br^-, OTf^-; 12-TMCO = 4,7,10-trimethyl-1-oxa-4,7,10-triazacyclododecane) and $S = 1$ $[Fe^{IV}(12\text{-TMCO})(O)(CH_3CN)]^{2+}$ complexes supported by the macrocyclic 12-TMCO ligand involving a N_3O coordination. In particular, the ligand donation

[a]*Institut für Chemie, Humboldt-Universitat zu Berlin, Brook-Taylor-Straße 2, 12489 Berlin, Germany. E-mail: kallol.ray@chemie.hu-berlin.de*

[b]*Department of Inorganic and Physical Chemistry, Indian Institute of Science, Bangalore, Karnataka-560012, India*

[c]*Department of Physics, Freie Universität Berlin, Arnimallee 14, 14195 Berlin, Germany*

[d]*Institut für Chemie, Technische Universität Berlin, Fakultät II, Straße des 17. Juni 135, 10623 Berlin, Germany*

† Electronic supplementary information (ESI) available: Experimental section; synthesis, characterization, and DFT details. CCDC 2296883. For ESI and crystallographic data in CIF or other electronic format see DOI: https://doi.org/10.1039/d3sc05603a

from the *cis*-anionic ligands like chloride or aryl thiolates and the H-bonding interaction mediated by 12-TMCO are shown to be prerequisites for the stabilization of $[Fe^{III}(12\text{-TMCO})(OOR)L']^+$. The present study provides a rationale for the presence of a *cis*- (rather than the speculated *trans*-) thiolate ligation in SOR and highlights the importance of subtle electronic changes in the stability and reactivity of the biologically relevant metal–dioxygen intermediates.

Results and discussion

Combining the tetradentate 12-TMCO ligand with $Fe(OTf)_2(CH_3CN)_2$ yielded the iron(II) precursor complex $[Fe^{II}(12\text{-TMCO})(OTf)_2]$ (**1**-$(OTf)_2$). The X-ray structure of **1**-$(OTf)_2$ (Scheme 1, inset) displays a distorted octahedral geometry with two *cis*-positions occupied by anionic triflate ($-OTf^-$) ligands. Notably, the smaller ring size of the 12-TMCO ligand forces the iron(II) center out of the equatorial plane involving the three nitrogen atoms of 12-TMCO and an oxygen atom of one of the $-OTf^-$ ligands. The etheral oxygen atom of 12-TMCO and the second –OTf ligand occupy the axial binding sites. The macrocyclic ring adopts a conformation in which all of the methyl groups are arranged *cis* to the axial $-OTf^-$ ligand, with iron–ligand bond lengths (Table S1a; for crystallographic information see Table S1b; ESI†) typical of a high-spin (HS) iron(II) complex. The zero-field Mössbauer spectrum of **1**-$(OTf)_2$ (Fig. S1†) revealed a single doublet with an isomer shift (δ) of 1.17 mm s^{-1} and a large quadrupole splitting (ΔE_Q) of 3.38 mm s^{-1}, which is also consistent with the presence of HS $S = 2$ Fe(II) center in **1**-$(OTf)_2$. In CH_3CN solution, the two $-OTf^-$ ligands are replaced by CH_3CN to form **1**-$(CH_3CN)_2$, as evident from ^{19}F-NMR (Fig. S2†) and extended X-ray absorption fine structure (EXAFS) measurements performed on a solution of **1**-$(OTf)_2$ in CH_3CN (Fig. S3b and c, Table S2†). A chloride-bound complex, **1**-Cl was also synthesized combining $FeClBF_4$ with 12-TMCO (Experimental section, ESI).† The formation of **1**-Cl was structurally confirmed by X-ray absorption studies (XAS) (Fig. S3†). EXAFS analysis of a solution of **1**-Cl in CH_3CN, (Fig. S3b, c and Table S2†) revealed close to one Cl scatterer at 2.32 Å and a further shell of three N and one O scatterers at 2.14 and 2.04 Å, respectively (corresponding to the N/O donors of 12-TMCO).

The reaction of **1**-$(CH_3CN)_2$ with excess ^{t}BuOOH in CH_3CN at −20 °C affords a light green chromophore (**2**; $t_{1/2}$ = 1.5 h at −20 °C) with absorption maxima (λ_{max}) centered at 770 nm (ε = 142 M^{-1} cm^{-1}) and 935 nm (ε = 170 M^{-1} cm^{-1}). The conversion of **1**-$(CH_3CN)_2$ to **2** takes place *via* the intermediate formation of a transient species **3**-CH_3CN with $\lambda_{max} \approx 517$ nm (Fig. 1a). Further characterizations of **2** were carried out by a variety of spectroscopic methods. The zero-field Mössbauer spectrum of **2** (Fig. 1b; $\Delta E_Q = 1.37$ mm s^{-1}, $\delta = 0.01$ mm s^{-1}) is consistent with the presence of an Fe^{IV} center in the $S = 1$ ground-state. Analysis of the EXAFS data of **2** in CH_3CN solution (Fig. S3b and c, Table S2†) yields about one oxygen ligand at 1.64 Å (assigned to the Fe=O unit) aside from the 4 further N/O ligands (at ∼2.05 Å and ∼1.90 Å) of the 12-TMCO group. The Fe K-edge spectrum of **2** (Fig. 2a) reveals a pronounced pre-edge amplitude at *ca.* 7114.3 eV and a K-edge energy of 7124.3 eV, which are typical for Fe^{IV}=O complexes.[22–27] The resonance Raman (rR) spectrum obtained with 406 nm excitation exhibits a band at 861 cm^{-1}, assigned to the Fe=O stretching mode [ν(Fe=O)] (Fig. S4† and 2c). This band disappears upon decay of **2** (data not shown).[28] Thus, in the absence of any anionic ligation, the HS Fe^{II} center in **1**-$(CH_3CN)_2$ performs O–O bond homolysis to yield an $[Fe^{IV}(TMCO)(O)(CH_3CN)]^{2+}$ complex **2**, presumably *via* the transient formation of $[Fe^{III}(TMCO)(OO^tBu)(CH_3CN)]^{2+}$ (**3**-CH_3CN). The homolytic O–O bond cleavage mechanism is further confirmed in the reaction of **1**-$(CH_3CN)_2$ in CH_3CN at −20 °C with cumenehydroperoxide (CumOOH), which is often used as a mechanistic probe.[29–33] Complex **2** is obtained in near-stoichiometric yield in the reaction (Fig. S5†) and the gas chromatographic analysis revealed the formation of acetophenone (Fig. S6†) confirming the homolytic O–O bond cleavage

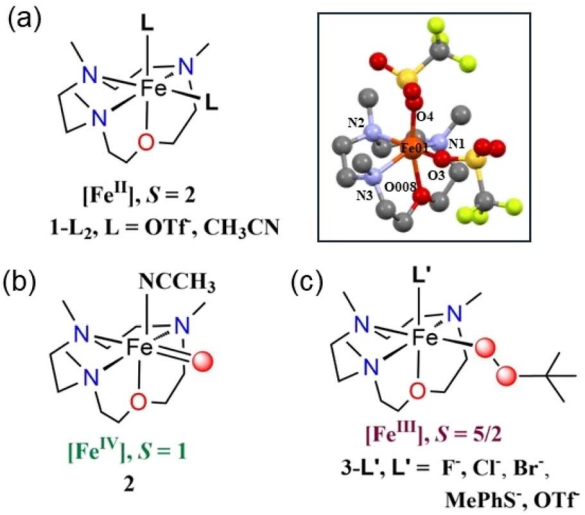

Scheme 1 Representative chemical structures of the species (a) **1**-L_2, (b) **2**, and (c) **3**-L′. Inset shows the XRD-determined molecular structure of **1**-$(OTf)_2$. Hydrogen atoms are removed for clarity. The selected bond distances: Fe–N(1) = 2.215(3) Å, Fe–N(2) = 2.223(3) Å, Fe–N(3) = 2.196(3) Å, Fe–O(008) = 2.167(2) Å, Fe–O(3) = 2.131(2) Å, Fe–O(4) = 2.045(2) Å. See Table S1a† for detailed bond lengths and bond angles. Color code: C: gray; N: blue; O: red; Fe: orange.

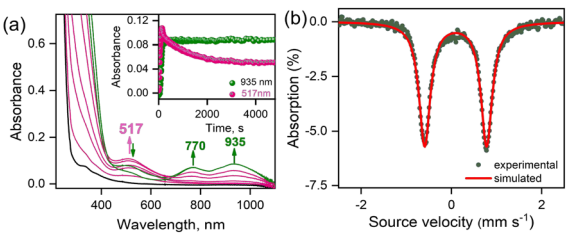

Fig. 1 (a) UV-visible spectral changes observed in the formation of **2** (green line) after the oxidation of **1**-$(CH_3CN)_2$ (0.50 mM, black line) by ^{t}BuOOH (20 equiv.) in CH_3CN at 253 K. The intermediate spectra are shown in pink. Inset shows the time profiles monitored at 935 nm due to the formation of **2** and at 517 nm for the concomitant formation and decay of the preequilibrium species **3**-CH_3CN. (b) The zero-field Mössbauer spectrum of **2** with isomer shift, δ = 0.01 mm s^{-1} and quadrupole splitting, $\Delta E_Q = 1.37$ mm s^{-1} recorded at 4.2 K in CH_3CN.

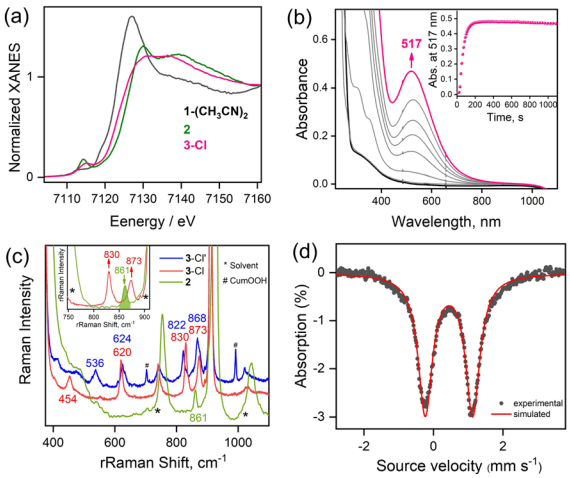

Fig. 2 (a) X-ray absorption near edge structure (XANES) spectra of solutions of **1**-$(CH_3CN)_2$, **2** and **3**-Cl in CH_3CN. (b) UV-visible spectral changes observed due to the formation of **3**-Cl after the reaction of **1**-$(CH_3CN)_2$ (0.50 mM) with ^{t}BuOOH (20 equiv.) in the presence of NEt_4Cl (5 equiv.) in CH_3CN at 253 K. Inset shows the time profile monitored at 517 nm due to the formation of **3**-Cl. (c) rRaman spectra of **3**-Cl synthesized with ^{t}BuOOH (red) and **3**-Cl′ synthesized with CumOOH (blue) upon laser irradiation at 514 nm in CH_3CN at −40 °C. The rRaman spectra of **2** synthesized with ^{t}BuOOH (green) using a 406 nm laser excitation in CH_3CN at −40 °C is shown for comparison. Inset shows the disappearance of rRaman band at 861 cm^{-1} for **2** (green) upon generation of **3**-Cl (red). (d) The zero-field Mössbauer spectrum of **3**-Cl with isomer shift, $\delta = 0.45$ mm s^{-1} and quadrupole splitting, $\Delta E_Q = 1.37$ mm s^{-1} recorded at 4.2 K.

mechanism.[29–33] No generation of cumylalcohol expected from O–O bond heterolysis was observed. DFT calculations on **2** (Fig. 3a, Table S3a†) predict an $S = 1$ ground-state with calculated Fe=O bond distance (1.60 Å), and stretching mode frequency (867 cm^{-1}), in good agreement with experiments (Table S4†).

Interestingly, the transient **3**-CH_3CN intermediate involved during the conversion of **1**-$(CH_3CN)_2$ to **2** can be stabilized in the presence of externally added anionic ligands. For example,

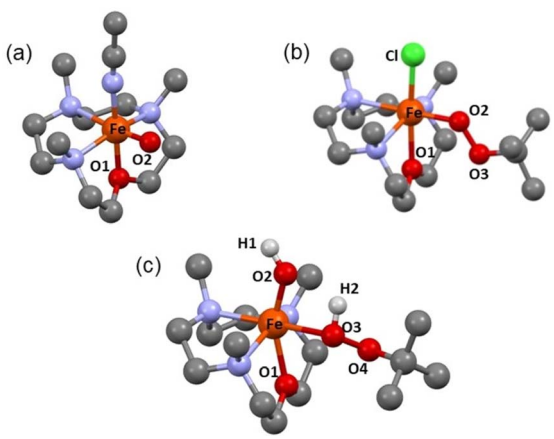

Fig. 3 DFT Optimized Structures of (a) **2**, (b) **3**-Cl and (c) **5**. The hydrogens are removed for clarity. See Tables S3a–c† for further information.

the reaction of **1**-$(CH_3CN)_2$ with excess ^{t}BuOOH in CH_3CN at −20 °C in the presence of NEt_4Cl results in the generation of a burgundy-colored species (**3**-Cl) with λ_{max} at 517 nm (ε = 880 M^{-1} cm^{-1}) (Fig. 2b). **3**-Cl is also generated in the direct reaction of **1**-Cl with ^{t}BuOOH at −20 °C in CH_3CN (Fig. S7†). Species **3**-Cl exhibits an EPR spectrum with signals at $g = 9.52$, and 4.3 that corresponds to a high-spin iron(III) ($S = 5/2$) center (Fig. S8†) and a rRaman spectrum with four resonance-enhanced vibrational modes at 536, 620, 830, and 873 cm^{-1} that arise from coordinated alkylperoxide[34] (Fig. 2c and Table S5†). Notably, these bands are significantly shifted in **3**-Cl′, involving a bound cumyl peroxide (–OOCum) ligand; **3**-Cl′ is generated in the reaction of **1**-$(CH_3CN)_2$ with excess CumOOH in CH_3CN at −20 °C in the presence of NEt_4Cl (Fig. 2c). This pattern of rRaman bands has been observed for high-spin alkylperoxoiron(III) intermediates and is distinct from that associated with their low-spin counterparts (Table S5†).[12–16,18,19] Further characterization of the Fe-center by zero-field Mössbauer analysis revealed a single doublet with an isomer shift (δ) of 0.45 mm s^{-1} and a quadrupole splitting $\Delta E_Q = 1.37$ mm s^{-1}, consistent with the HS Fe(III) assignment of **3**-Cl (Fig. 2d). XAS revealed an Fe K-edge energy of **3**-Cl in between the energies of **1**-$(CH_3CN)_2$ and **2** (Fig. 2a), supporting the Fe(III) assignment of **3**-Cl. The EXAFS analysis of **3**-Cl in a frozen CH_3CN solution (Fig. S3b and c, Table S2†) reveals a Fe–Cl scatterer at 2.26 Å, and three N (at 2.19 Å) and one O (at 2.04 Å) scatterers assignable to the 12-TMCO ligand. Furthermore, two distinct Fe–O shells, at 1.82 Å and 3.15 Å, respectively, confirm the end-on binding mode of –OO^{t}Bu in **3**-Cl. Thus **3**-Cl can be characterized as a high-spin $[Fe^{III}(12\text{-TMCO})(OO^tBu)(Cl)]^+$ ion. DFT calculations on **3**-Cl (Fig. 3b; Table S3b†) predict the presence of a distorted octahedral (O_h) Fe(III) center in an $S = 5/2$ ground-state. The three nitrogen donors of the 12-TMCO ligand and the –OO^{t}Bu moiety occupy the equatorial positions of the O_h, whereas the etheral oxygen atom and the chloride anion constitute the axial ligands. The calculated metrical parameters are in reasonable agreement with the experimental data (Table S6†). **3**-Cl did not exhibit any electrophilic hydrogen atom transfer (HAT) abilities even in the presence of substrates containing weak C–H bonds (for example xanthene and 1,4-cyclohexadiene). Similarly, it was found to be incapable of performing oxygen atom transfer (OAT) to triphenylphosphine. **3**-Cl also didn't show any nucleophilic reactivity with substrates like 2-phenylpropionaldehyde.

Parallel reactions using either F^-, Br^- or aryl thiolate ($MePhS^-$) anionic ligands yield intermediates **3**-F, **3**-Br, or **3**-SPhMe, respectively, with varying absorbance maxima (Fig. 4, Table S7†) depending on the anions used. In particular, the significant blue shift of the absorption band observed from **3**-Cl ($\lambda_{max} \approx 517$ nm) to **3**-SPhMe ($\lambda_{max} \approx 460$ nm) can be rationalized by the substitution of the axial chloride ligand in **3**-Cl with a more Lewis basic thiolate ligand in **3**-SPhMe and is consistent with the assignment of the chromophore as an alkylperoxo-to-iron(III) charge-transfer transition.[15] Notably, the reaction of **1**-$(OTf)_2$ with excess ^{t}BuOOH in a non-coordinating solvent like acetone, where the –OTf^- ligands stay bound to the Fe(II) center, also affords a deep purple chromophore with $\lambda_{max} = 510$ nm

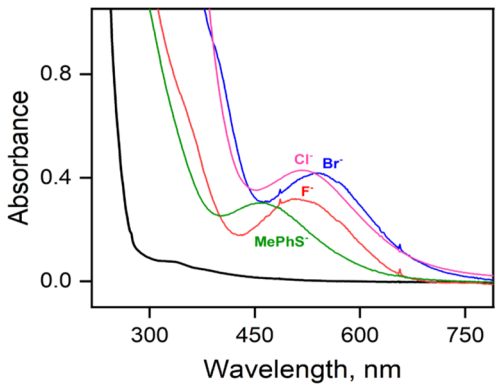

Fig. 4 UV-visible spectral changes observed due to the formation of **3**-L′ from the reaction of **1**-$(CH_3CN)_2$ (0.5 mM, black line) with ^{t}BuOOH (20 equiv.) in the presence of 5 equiv. sodium toluene-*p*-thiolate (NaSPhMe, green), tetramethylammonium fluoride (NMe_4F, red), tetrabutylammonium bromide (NBu_4Br, blue) and tetraethylammonium chloride (NEt_4Cl, pink), in CH_3CN at −20 °C.

corresponding to **3**-OTf (Fig. S9†). This is in contrast to the reaction in a coordinating solvent like CH_3CN whereby the Fe^{III}–OO^tBu species is transient and undergoes spontaneous O–O bond homolysis to yield the oxo–iron(IV) species. Thus, a *cis*-anionic ligand donation appears to stabilize the HS Fe^{III}–OO^tBu unit by retarding the O–O bond lysis step. The decay of **3**-Cl and **3**-SPhMe have been monitored at temperatures between −20 °C to +25 °C (Fig. S10†); no generation of the oxoiron(IV) species **2** by O–O bond homolysis has been observed.

The oxoiron(IV) complex **2** can, however, be converted to the Fe^{III}–OO^tBu species in the presence of excess ^{t}BuOOH and anionic ligands (Fig. S11†). For example, the addition of NEt_4Cl to a CH_3CN solution of **2** in the presence of excess ^{t}BuOOH at −20 °C leads to the immediate decay of the characteristic absorption bands of **2** at 770 nm and 935 nm, and the concomitant appearance of the band at 517 nm corresponding to **3**-Cl. Notably, the time trace of the decay of the 770 nm band showed a pseudo first-order dependence on the concentration of NEt_4Cl. In contrast, the rate of generation of **3**-Cl was found to be independent of the NEt_4Cl concentration. We therefore propose a mechanism where the conversion of **2** to **3**-Cl takes place *via* the intermediate formation of an Fe^{III}–OH species (**4**), which is generated by the decay of **2** in the presence of NEt_4Cl (Scheme S1†). The Fe^{III}–OH moiety, as suggested previously,[13,35] then reacts with ^{t}BuOOH to yield Fe^{III}–OO^tBu, which is stabilized by binding a *cis*-anionic chloride ligand. In contrast to chloride ligand, which led to a stoichiometric conversion of **2** to **3**-Cl, other anions like F^- or Br^- did not lead to a clean conversion, presumably because of the lower stabilities of **3**-Br and **3**-F compared to **3**-Cl (Fig. S12†).

The N_3O macrocycle in 12-TMCO is found to be a prerequisite for the stabilization of Fe^{IV}=O or Fe^{III}–OO^tBu cores in reactions of the (12-TMCO)Fe^{II} compounds with ^{t}BuOOH. Notably, the corresponding iron(II) compound based on the N_4 macrocycle $[Fe^{II}(12\text{-TMC})(CH_3CN)_2]^{2+}$ (**8**) (12-TMC = 1,4,7,10-tetramethyl-1,4,7,10-tetraazacyclododecane)[36] yields an Fe_2O_3 precipitate and free ligand in its reaction with excess ^{t}BuOOH. Although, both **1**-$(CH_3CN)_2$ and $[Fe^{II}(12\text{-TMC})(CH_3CN)_2]^{2+}$ contain *cis*-labile binding sites, the different products formed in their reactions with ^{t}BuOOH is presumably attributed to the different reactivities of their iron(III)hydroxide complexes, which are plausible intermediates necessary for the generation of the Fe^{III}–OO^tBu core.[13,35] DFT calculations reveal that the transition state leading to the formation of **2** is preceded by an intermediate $[Fe^{III}(12\text{-TMCO})(OH)(HOO^tBu)]^{2+}$ (**5**; Scheme 2 and Fig. 3c), where the axial hydroxide donor is involved in

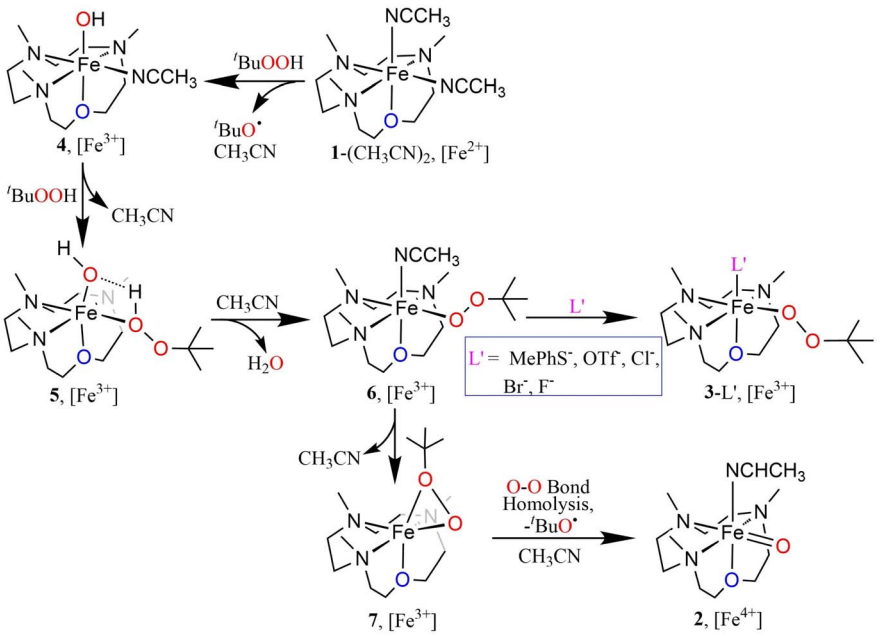

Scheme 2 Schematic representation of the proposed reaction mechanism.

hydrogen-bonding interaction with ^{t}BuOOH (Fig. S13a†), thereby making ^{t}BuOOH binding and the subsequent release of water to form **3**-L′ (in the presence of anionic ligands), highly exergonic. Notably, our efforts to optimize the corresponding Fe^{III}(12-TMC)(OH)(HOO^{t}Bu)]$^{2+}$ complex involving the N_4 macrocycle resulted in the loss of the ^{t}BuOOH fragment in the calculation (Fig. S13b, Table S3d†); so no H-bonding mediated binding of ^{t}BuOOH to [Fe^{III}(12-TMC)(OH)]$^{+}$ is possible, and the latter decays to form Fe_2O_3 and free ligand.

Conclusion

In summary, in the present study, we have demonstrated the importance of *cis*-anionic ligand donations (including the thiolate relevant to SOR) for the stabilization of HS iron(III)–peroxo complexes. These results contrast the previously reported "push" effect[11,14] that promotes O–O bond cleavage in HS and LS iron(III) peroxo complexes. The current study provides a basis to discuss the function of the high-spin {$Fe^{II}(His)_4(Cys)$} active site of SOR. Although the putative O_2-binding site is considered *trans*- to the axial thiolate ligand,[6,8,9] the redox induced structural changes at the level of the peptide bond(s), as previously demonstrated by one of us and others,[37,38] may lead to the formation of a HS *cis*-[Fe^{III}(OOH)(Cys)]$^{+}$ moiety. The O–O bond cleavage to produce the undesired high-valent oxo–iron species is presumably prevented by the high-spin iron(III) center and the presence of the equatorial thiolate ligand. Furthermore, the importance of secondary interactions in the stabilization of [Fe^{III}–OO^{t}Bu] moiety, may also attribute to increasing the lifetime of the peroxo–iron(III) species in SOR to allow its protonation by a second-sphere residue and subsequent release of H_2O_2. The demonstrated contrasting effects of *cis*- and *trans*-anionic ligands on the fate of the HS Fe^{III}–OO^{t}Bu moiety may, therefore, provide a rationale for nature's use of axial- and equatorial-thiolate ligations in P-450 and SOR, respectively, for two apparently distinct roles.

Data availability

The data underlying this study, which are not included in the main text are available in the ESI.† The source data files can be provided upon request.

Author contributions

TD, KD, JD contributed in the experimental work and SM contributed in DFT calculations. UK and PH contributed in rRaman measurements and analysis of the data. MH and HD contributed in carrying out XAS studies. BC recorded the crystallographic data. KR and TD initiated the project and wrote the manuscript.

Conflicts of interest

There are no conflicts to declare.

Acknowledgements

This work was funded by Alexander-von-Humboldt (AvH) Postdoctoral Research Fellowship from AvH Research foundation, Germany to T. D. and K. D. was funded by the Einstein Foundation Berlin. We thank the Deutsche Forschungsgemeinschaft (DFG; German Research Foundation) for EXC-2008—390540038—"UniSysCat". We acknowledge the Helmholtz Zentrum Berlin (HZB) for allocating beamtime at beamline KMC-3 of the BESSY synchrotron and I. Zizak (HZB) for experimental support. H. D. and M. H. thank the German Bundesministerium für Bildung und Forschung (BMBF) for funding (Grant 05K22KE1, life-XAS).

Notes and references

1 L. Que Jr and R. Y. N. Ho, *Chem. Rev.*, 1996, **96**, 2607.
2 I. G. Denisov, T. M. Makris, S. G. Sligar and I. Schlichting, *Chem. Rev.*, 2005, **105**, 2253.
3 J. Rittle and M. T. Green, *Science*, 2010, **330**, 933.
4 S. Shaik, S. Cohen, Y. Wang, H. Chen, D. Kumar and W. Thiel, *Chem. Rev.*, 2010, **110**, 949.
5 E. G. Kovaleva, M. B. Neibergall, S. Chakrabarty and J. D. Lipscomb, *Acc. Chem. Res.*, 2007, **40**, 475.
6 A. P. Yeh, Y. Hu, F. E. Jenney Jr, M. W. W. Adams and D. C. Rees, *Biochemistry*, 2000, **39**, 2499.
7 K. Auclair, P. Moënne-Loccoz and P. R. O. de Montellano, *J. Am. Chem. Soc.*, 2001, **123**, 4877.
8 J. P. Emerson, E. D. Coulter, R. S. Phillips and D. M. Kurtz, *J. Biol. Chem.*, 2003, **278**, 39662.
9 T. Kitagawa, A. Dey, P. Lugo-Mas, J. B. Benedict, W. Kaminsky, E. I. Solomon and J. A. Kovacs, *J. Am. Chem. Soc.*, 2006, **128**, 14448.
10 A. A. A. A. Attia, D. Cioloboc, A. Lupan and R. Silaghi-Dumitrescu, *J. Biol. Inorg. Chem.*, 2013, **18**, 95.
11 J. Kaizer, M. Costas and L. Que Jr, *Angew. Chem., Int. Ed.*, 2003, **42**, 3671.
12 Y. Zang, J. Kim, Y. Dong, E. C. Wilkinson, E. H. Appelman and L. Que Jr, *J. Am. Chem. Soc.*, 1997, **119**, 4197.
13 M. R. Bukowski, H. L. Halfen, T. A. van den Berg, J. A. Halfen and L. Que Jr, *Angew. Chem.*, 2005, **117**, 590.
14 S. Hong, Y.-M. Lee, K.-B. Cho, M. S. Seo, D. Song, J. Yoon, R. Garcia-Serres, M. Clémancey, T. Ogura, W. Shin, J.-M. Latour and W. Nam, *Chem. Sci.*, 2014, **5**, 156.
15 F. Namuswe, T. Hayashi, Y. Jiang, G. D. Kasper, A. A. N. Sarjeant, P. Moënne-Loccoz and D. P. Goldberg, *J. Am. Chem. Soc.*, 2010, **132**, 157.
16 N. Lehnert, R. Y. N. Ho, L. Que Jr and E. I. Solomon, *J. Am. Chem. Soc.*, 2001, **123**, 8271.
17 H. Jeon and S. Hong, *Chem. Lett.*, 2019, **48**, 80.
18 L. R. Widger, Y. Jiang, A. C. Mc Quilken, T. Yang, M. A. Siegler, H. Matsumura, P. Moënne-Loccoz, D. Kumar, S. P. de Visser and D. P. Goldberg, *Dalton Trans.*, 2014, **43**, 7522.
19 T.-C. Yang, R. L. Mc Naughton, M. D. Clay, F. E. Jenney Jr, R. Krishnan, D. M. Kurtz Jr, M. W. W. Adams,

M. K. Johnson and B. M. Hoffman, *J. Am. Chem. Soc.*, 2006, **128**, 16566.
20 D. Krishnamurthy, G. D. Kasper, F. Namuswe, W. D. Kerber, A. A. N. Sarjeant, P. Moënne-Loccoz and D. P. Goldberg, *J. Am. Chem. Soc.*, 2006, **128**, 14222.
21 F. Namuswe, G. D. Kasper, A. A. N. Sarjeant, T. Hayashi, C. M. Krest, M. T. Green, P. Moënne-Loccoz and D. P. Goldberg, *J. Am. Chem. Soc.*, 2008, **130**, 14189.
22 X. Huang and J. T. Groves, *Chem. Rev.*, 2018, **118**, 2491.
23 R. A. Baglia, J. P. T. Zaragoza and D. P. Goldberg, *Chem. Rev.*, 2017, **117**, 13320.
24 X. Engelmann, I. Monte-Perez and K. Ray, *Angew. Chem., Int. Ed.*, 2016, **55**, 7632.
25 M. Puri and L. Que Jr, *Acc. Chem. Res.*, 2015, **48**, 2443.
26 J.-U. Rohde, A. Stubna, E. L. Bominaar, E. Münck, W. Nam and L. Que Jr, *Inorg. Chem.*, 2006, **45**, 6435.
27 M. Guo, T. Corona, K. Ray and W. Nam, *ACS Cent. Sci.*, 2019, **5**, 13.
28 Due to the non-availability of 18-O labelled ^{t}BuOOH and the decay of **2** in presence of 18-O labelled H_2O synthesis of ^{18}O labelled **2** was not possible. Notably, complex **2** can also be generated in presence of CumOOH (Fig. S4†) and shows a Fe=O vibration at 861 cm^{-1}.
29 T. Tano, H. Sugimoto, N. Fujieda and S. Itoh, *Eur. J. Inorg. Chem.*, 2012, 4099.
30 A. Kunishita, H. Ishimaru, S. Nakashima, T. Ogura and S. Itoh, *J. Am. Chem. Soc.*, 2008, **130**, 4244.
31 S. Adachi, S. Nagano, K. Ishimori, Y. Watanabe, I. Morishima, T. Egawa, T. Kitagawa and R. Makino, *Biochemistry*, 1993, **32**, 241.
32 D. V. Avila, C. E. Brown, K. U. Ingold and J. Lusztyk, *J. Am. Chem. Soc.*, 1993, **115**, 466.
33 E. Baciocchi, M. Bietti, M. Salamone and S. Steenken, *J. Org. Chem.*, 2002, **67**, 2266.
34 N. Lehnert, R. Y. N. Ho, L. Que Jr and E. I. Solomon, *J. Am. Chem. Soc.*, 2001, **123**, 12802.
35 A. L. Balch, *Inorg. Chim. Acta*, 1992, **198–200**, 297–307.
36 W. Zhu, A. Kumar, J. Xiong, M. J. Abernathy, X.-X. Li, M. S. Seo, Y.-M. Lee, R. Sarangi, Y. Guo and W. Nam, *J. Am. Chem. Soc.*, 2023, **145**, 4389.
37 C. Berthomieu, F. Dupeyrat, M. Fontecave, A. Verméglio and V. Nivière, *Biochemistry*, 2002, **41**, 10360.
38 M. Horsch, T. Utesch, P. Hildebrandt, M. A. Mroginski and I. Zebger, *Phys. Chem. Chem. Phys.*, 2016, **18**, 23053.